Toxicology Reports 12 (2024) 1–9

Contents lists available at ScienceDirect

Toxicology Reports

journal homepage: www.elsevier.com/locate/toxrep

Non-invasive differentiation of hepatic steatosis and steatohepatitis in a mouse model using nitroxyl radical as an MRI-contrast agent

Yuka Yoshino [a,b,*], Yuta Fujii [a,b], Kazuhiro Chihara [a], Aya Nakae [b,c], Jun-ichiro Enmi [b,c], Yoshichika Yoshioka [b,c], Izuru Miyawaki [a]

[a] Preclinical Research Unit, Sumitomo Pharma Co., Ltd., 3-1-98 Kasugade-naka, Konohana-ku, Osaka 554-0022, Japan
[b] Graduate School of Frontier Biosciences, Osaka University, 1-3 Yamadaoka, Suita city, Osaka 565-0871, Japan
[c] Center for Information and Neural Networks (CiNet), Osaka University and National Institute of Information and Communications Technology (NICT), 1-4 Yamadaoka, Suita City, Osaka 565-0871, Japan

ARTICLE INFO

Handling Editor: Prof. L.H. Lash

Keywords:
Steatohepatitis
Magnetic resonance imaging
Nitroxyl radicals
Reactive oxygen species

ABSTRACT

Drug-induced steatohepatitis is considered more serious than drug-induced hepatic steatosis, so that differentiating between the two is crucial in drug development. In addition, early detection of drug-induced steatohepatitis is considered important since recovery is possible with drug withdrawal. However, no method has been established to differentiate between the two. In the development of drug-induced steatohepatitis, reactive oxygen species (ROS) is excessively generated in the liver. It has been reported that ROS can be monitored with electron spin resonance (ESR) and dynamic nuclear polarization-magnetic resonance imaging (DNP-MRI) by using nitroxyl radicals, which are known to participate in various in vivo redox reactions. The decay/reduction rate, which is an index for monitoring nitroxyl radicals, has been reported to be increased in tissues with excessive ROS levels other than liver, but decreased in methionine choline deficient (MCD) diet-induced steatohepatitis with excess ROS. Therefore, looking to differentiate between drug-induced hepatic steatosis and steatohepatitis, we examined whether the reduction rate decreases in steatohepatitis other than the MCD-diet induced disease and whether the decrease could be detected by MRI. We used STAM™ mice in which hepatic steatosis and steatohepatitis developed sequentially under diabetic conditions. 3-carbamoyl-PROXYL (CmP), one of the nitroxyl radicals, was injected intravenously during the MRI procedure and the reduction rate was calculated. The reduction rate was significantly higher in early steatohepatitis than in hepatic steatosis and the control. Excess ROS in early steatohepatitis was detected by an immunohistochemical marker for ROS. Therefore, it was indicated that the increase or decrease in the reduction rate in steatohepatitis differs depending on the model, and early steatohepatitis could be noninvasively differentiated from hepatic steatosis using CmP in MRI. Since the change in direction of the reduction rate in steatohepatitis in clinical studies could be predicted by confirming the reduction rate in preclinical studies, the present method, which can be used consistently in clinical and preclinical studies, warrants consideration as a candidate monitoring method for differentiating between early drug-induced steatohepatitis and hepatic steatosis in drug development.

1. Introduction

Although both hepatic steatosis and steatohepatitis are characterized by lipid accumulation in hepatocytes, only steatohepatitis is associated with liver inflammation. Hepatic steatosis and steatohepatitis are induced by drugs, such as amiodarone, tamoxifen, and valproic acid

Abbreviations: ROS, reactive oxygen species; ESR, electron spin resonance; DNP-MRI, dynamic nuclear polarization-magnetic resonance imaging; MCD, methionine choline deficient; CmP, 3-carbamoyl-PROXYL; MRI, magnetic resonance imaging; PBS, phosphate buffered saline; CNR, contrast-to-noise ratio; FLASH, fast low-angle shot; TR, repetition time; TE, echo time; FA, flip angle; FOV, field of view; ROI, regions of interest; HE, hematoxylin and eosin; NASH, non-alcoholic steatohepatitis; RARE, rapid acquisition with relaxation enhancement; AUC, area under the hepatic signal intensity change rate-time curve; NAFLD, non-alcoholic fatty liver disease; NAS, NAFLD Activity Score; SAF-A score, the activity part of the Steatosis, Activity, and Fibrosis score; 4-HNE, 4-hydroxynonenal; USPIOs, ultrasmall superparamagnetic iron oxide particles.

* Corresponding author at: Preclinical Research Unit, Sumitomo Pharma Co., Ltd., 3-1-98 Kasugade-naka, Konohana-ku, Osaka 554-0022, Japan.
E-mail address: yuka.yoshino@sumitomo-pharma.co.jp (Y. Yoshino).

https://doi.org/10.1016/j.toxrep.2023.12.002
Received 27 July 2023; Received in revised form 5 December 2023; Accepted 7 December 2023
Available online 9 December 2023

[21] and sometimes observed in preclinical toxicology studies of drug candidates. Hepatic steatosis is typically regarded as benign with toxicologically non-adverse findings [2,18]. On the other hand, steatohepatitis is an adverse finding with tissue injury, and the chronic inflammatory state in steatohepatitis may progress to fibrosis, cirrhosis, and hepatocellular carcinoma [5]. For this reason, steatohepatitis is considered to be more serious than hepatic steatosis [37], and to differentiate between these two clinically is important and required for drug development. In addition, recovery from drug-induced steatohepatitis is known to occur with drug withdrawal in an early stage of the disease [30,35]. Therefore, it is important to monitor the difference between hepatic steatosis and steatohepatitis in order to determine whether the subject's safety can be ensured by drug withdrawal. In clinical use, the biopsy remains the gold standard for differentiating between steatohepatitis and hepatic steatosis [3]. Several limitations of biopsy make it unsuitable as a monitoring method for differentiating between the two, and no monitoring methods have been established. Limitations in the biopsy method include its invasiveness, which prevents it from being performed multiple times, and restriction to only a portion of heterogeneous liver lesions, which may lead to underestimation of the heterogeneity of the lesions. Imaging is a method that overcomes these limitations, but although methods of lipid evaluation have been established [6], methods of inflammation evaluation have not.

In the development of drug-induced steatohepatitis, disturbance of mitochondrial function is thought to play a critical role. Mitochondrial toxicity can lead to the release of reactive oxygen species (ROS) [38]. In fact, it has been reported that ROS are generated in the liver by drugs that induce steatohepatitis, such as irinotecan, methotrexate, valproic acid, amiodarone, and oxaliplatin in experiments using animals and HepG2 cells [1,10,22,23]. ROS and inflammation interact in a vicious cycle of reciprocal reinforcement [11,24]. This is consistent with reports that ROS has been generated more in steatohepatitis than in hepatic steatosis [33,39]. Therefore, we considered that excess ROS could be the biomarker to differentiate between drug-induced hepatic steatosis and steatohepatitis in both clinical and nonclinical studies.

Imaging of ROS using nitroxyl radicals as probe and contrast agent has been reported in animal studies using electron spin resonance (ESR) and dynamic nuclear polarization-magnetic resonance imaging (DNP-MRI), respectively [13,14,29,43]. Nitroxyl radicals are involved in various in vivo redox reactions, including oxidation by ROS, and are finally converted to hydroxylamine which doesn't have an unpaired electron [41] (Fig. 1). In ESR which detects the electron spin signals, this conversion can be observed as a gradual decay of signal. The rate of this signal change is called the decay rate. In magnetic resonance imaging (MRI) which observes nuclear spin, this conversion can be observed as a gradual reduction of signal intensity on T1-weighted MRI. This is because unpaired electron affects the T1-relaxation of water protons. The rate of this signal intensity change is called the reduction rate. It has been reported that the decay rate of nitroxyl radicals was enhanced in conditions associated with excess ROS, such as gastric ulcers, septic condition of the head, and focal muscle inflammation in ESR [13,14,43]. However, compared to normal or hepatic steatosis, steatohepatitis induced by methionine choline deficient (MCD) diet showed a decrease in the reduction rate of nitroxyl radicals monitored by DNP-MRI [29]. It is unclear whether the decay/reduction rate in other steatohepatitis models would also decrease, and whether this rate change for steatohepatitis could be detected in MRI, which can be used consistently in clinical and preclinical studies.

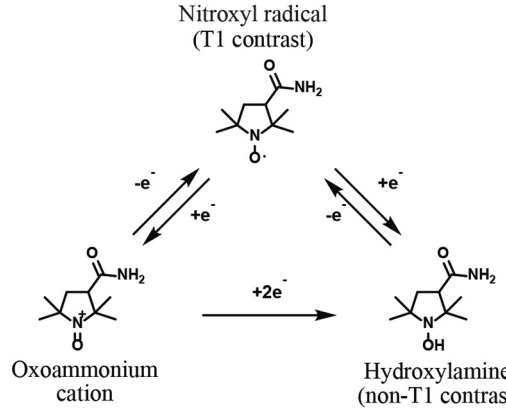

Fig. 1. Redox transformation of the nitroxyl radical. The nitroxyl radical is converted to hydroxylamine by reduction or by oxidation to an oxoammonium cation and further reduction. Those conversions are reversible and the equilibrium between the nitroxyl radical and hydroxylamine occurs after in vivo administration. The nitroxyl radical provides T1 contrast because it has an unpaired electron. The hydroxylamine doesn't provide T1 contrast because it doesn't have an unpaired electron.

The purpose of this study was thus, looking to differentiate between drug-induced hepatic steatosis and steatohepatitis, to verify whether the reduction rate is decreased in steatohepatitis models other than the MCD-diet induced model, and whether this change could be detected by MRI.

2. Material and methods

2.1. Animal

In animal study, male STAM™ mice was used as hepatic steatosis and steatohepatitis models (SMC Laboratories, Inc., Tokyo, Japan). STAM™ mice were made by administering streptozotocin to 2-day-old C57BL/6J mice and feeding them a high fat diet from 4 weeks of age. This mouse models the sequential progression of disease from the fatty liver disease, non-alcoholic steatohepatitis (NASH), to fibrosis to hepatocellular carcinoma under diabetic conditions [15]. Male C57BL/6J mice was used as controls.

2.2. MRI

All MRI examinations were performed on an 11.7T vertical-bore Bruker Avance II imaging system (Bruker BioSpin, Ettlingen, Germany) with a volume radiofrequency coil for transmission and reception (m2m Imaging Corp., Cleveland, OH, USA).

2.3. Chemicals

We selected 3-carbamoyl-PROXYL (CmP) (Sigma-Aldrich, St. Louis, MO, USA) among nitroxyl radicals. This was because CmP was cell permeable and so suitable for detecting ROS generated in cells. CmP was diluted with phosphate buffered saline (PBS) pH 7.4.

2.4. Phantom study design

A phantom is an object for optimizing imaging parameters and checking the performance of contrast agent and imaging equipment such as X-ray, MRI, and ultrasound machines, without using a living body. The present phantom study was conducted to calculate the contrast-to-noise ratio (CNR) and predict whether the planned dose 200 mg/kg, which previous reports [25,27] indicated was non-toxic, would provide sufficient contrast to distinguish the phantom from the background on an 11.7 T MRI. In addition, the relaxivity, which represents the ability as a contrast agent, was measured, and the method and result were included in the supplemental data. The prediction of CNR at the planned dose was necessary because the ability of CmP as a contrast agent was lower than that of commonly used Gd contrast agent, as shown in the supplemental data, and the use of CmP at high magnetic fields has not been reported. After predicting that nitroxyl radical could have sufficient signal intensity in animals, we conducted the animal

study.

2.4.1. Phantom

The phantom consisted of 12 disposable capillary pipettes (ringcaps; internal diameter, 1.89 mm, Hirschmann Laborgeräte GmbH & Co. KG, Eberstadt, Germany) placed inside a polypropylene tube filled with PBS. The ringcaps contained 0, 0.5, 1, 2, 4, 6, 8, 10, 20, 30, 40, or 50 mM of CmP. Phantom experiments were repeated three times using freshly prepared samples.

2.4.2. MRI examination

T1-weighted images were acquired using fast low-angle shot (FLASH) with the following scanning parameters: repetition time (TR)/ echo time (TE) = 24 ms/1.32 ms, flip angle (FA) 30°, field of view (FOV) 20 mm × 20 mm, matrix of 128 × 128 pixels, slice with thickness = 1.5 mm, 4 NEX, and number of repetitions 1.

2.4.3. Analysis

The signal intensity at regions of interest (ROI) was measured by Image J (NIH, MD, USA). ROI was 0.9 mm^2 circle and positioned centrally in each ringcap. The CNR was determined by the equation below.

$$\mathrm{CNR} = \sqrt{\frac{\pi}{2}}\,\frac{[\mathrm{SI}(x) - \mathrm{SI}(0)\,]}{\mathrm{SI(air)}}\,\# \tag{1}$$

SI(x), SI(0), and SI(air) are signal intensities at the concentration to calculate CNR, 0 mM, and air, respectively. The CNR apparently distinguishable from background was defined as ≥ 5 [36].

2.5. Animal study design

2.5.1. Animal

All animal studies were approved by the Committee for the Ethical Usage of Experimental Animals of Sumitomo Pharma Co., Ltd. and the Animal Welfare Committee of Osaka University. Forty male STAM™ mice (5- and 8-week-old) as hepatic steatosis and steatohepatitis models were purchased from SMC Laboratories, Inc. (Tokyo, Japan), and twenty-four male C57BL/6J mice were purchased from Japan SLC, Inc. (Shizuoka, Japan). Nineteen STAM™ mice (5- and 8-week-old) and seven C57BL/6J mice (5- and 8-week-old) as controls were subjected to an MRI examination and twenty-one STAM™ mice (5- and 8-week-old) and seven C57BL/6J mice (5- and 8-week-old) as controls were subjected to immunohistochemical examination. Ten male C57BL/6J mice (7-week-old) were subjected to examine the in vivo safety of CmP. All animals were subjected to histopathological examination using hematoxylin and eosin (HE) stain.

2.5.2. MRI examination

All mice were fasted more than 12 h before MRI and/or histopathological examination. After the body weight measurements and tail vein cannulation, the mice were anesthetized with 1–2 % isoflurane (Wako, Osaka, Japan), and then placed in the MRI scanner. Respiration rate was monitored using a physiological monitoring system (SA Instruments, Stony Brook, NY), and body temperature was kept at 36.0 ± 0.5 °C by circulating water through heating pads. To determine the position of images with CmP, T2-weighted images through the liver in the coronal, axial, and sagittal planes were acquired using rapid acquisition with relaxation enhancement (RARE) with the following scanning parameters: Rare Factor 16, TR/TE 3000 msec/45 msec, FOV 25 mm × 25 mm, matrix of 256 × 256 pixels, 20 slices with thickness = 1.0 mm, and 8 NEX. T1-weighted images with CmP through the liver in the coronal planes were acquired using FLASH with parameters similar to those used in the phantom study: TR/TE 24 msec/1.5 msec, FA 30°, FOV 20 mm × 20 mm, matrix of 128 × 128 pixels, 1 slice with thickness = 1.5 mm, 4 NEX, and number of repetitions 102. Images with CmP were acquired for 17 min at 10-second intervals. The dose, 200 mg/kg, of CmP was administered intravenously 2 min after starting data acquisition. In addition, to assess hepatic blood flow, Gd HP-DO3A (ProHance, Eisai, Tokyo, Japan) was dosed intravenously 30 min after CmP dosing in one 8-week-old STAM™ mouse with partial hyperintensity in T2-weighted MRI as described below and one 8-week-old C57BL/6 J mouse.

2.5.3. MRI analysis

The signal intensity at the ROI was measured by Image J. In order to examine whether ROS can be detected in an organ specific manner, ROIs were placed in areas of the liver and stomach that were less affected by body movement. ROIs were placed with care to avoid major blood vessels and other tissue with reference to T2-weighted images. The areas of the ROIs at the liver and stomach were set to 1.27 mm^2 and 0.29 mm^2, respectively, which were the approximate maximum areas ensuring no overlap with large blood vessels and other tissue. The reduction rate of signal intensity exerted by CmP affecting T1-relaxation of water proton was calculated from the slope of the linear regression line of the semilogarithmic plot of signal intensity change rate against time, for 5.83 min after the peak. Signal intensity change rate was calculated by dividing the signal intensity at a time point minus the average pre-dose signal intensity by the average pre-dose signal intensity. In addition, the signal intensity in each pixel was measured by Image J and the reduction rates in each pixel were calculated in representative mice. The reduction rates in each pixel were re-imaged. Reduction rate in stomach could not be calculated in some animals in all groups due to body movement effects. To assess hepatic blood flow, the area under the hepatic signal intensity change rate-time curve (AUC) for Gd HP-DO3A was preliminarily determined for 50 s, 80 s, 170 s, and 290 s after dosing. The same ROIs as in CmP image analysis were used in Gd HP-DO3A image analysis.

2.5.4. In vivo safety examination of CmP

Ten C57BL/6J mice were divided into vehicle (PBS) and CmP 200 mg/kg group each with five mice. Vehicle or CmP were administered via tail vein at once. On the day of the administration, blood was withdrawn from the caudal vena cava under isoflurane anesthesia for blood biochemistry, and the mice were euthanized. Blood placed in polypropylene tubes containing heparin lithium was centrifuged to obtain plasma. Aspartate aminotransferase, alanine transaminase, alkaline phosphatase, lactate dehydrogenase, total bilirubin, γ-glutamyl transpeptidase, creatine kinase, total cholesterol, phospholipid, triglycerides, glucose, blood urea nitrogen, creatinine, phosphorus, calcium, sodium, potassium, chloride, total protein, albumin, and albumin/ globulin were determined by using an automated analyzer JCA-ZS050 (JEOL Ltd., Tokyo, Japan).

2.5.5. Histopathological examination and analysis

In the MRI and immunohistochemical examination, the livers and/or stomachs were fixed in 10 % neutral-buffered formalin. In in vivo safety examination of CmP, liver, kidney, heart, lung, brain, and administration site (tail) were fixed in 10 % neutral-buffered formalin. These organs were embedded in paraffin, sectioned, stained with HE, and examined by light microscopy. The severity of steatohepatitis was evaluated using the non-alcoholic fatty liver disease (NAFLD) Activity Score (NAS). The NAS is the total score including the subscores for steatosis (0–3), lobular inflammation (0–3), and ballooning (0–2). NASs of < 3, 3–4, and ≥ 5 are judged as non-NASH, borderline, and NASH, respectively [20]. According to the histopathological examination, STAM™ mice were divided into the hepatic steatosis, steatohepatitis (NAS of 2), and steatohepatitis (NAS of 3) groups. For reference, severity of steatohepatitis was also evaluated based on the activity part of the Steatosis, Activity, and Fibrosis score (SAF-A score). The grade of activity was calculated by addition of grades of ballooning and lobular inflammation.

In addition, immunohistochemistry using 4-hydroxynonenal (4-

HNE) antibody (Japan Institute for the Control of Aging, Shizuoka, Japan), which is lipid peroxidation marker, was conducted to examine excess ROS generation in the liver. Nitroxyl radicals including CmP have been known to have a therapeutic effect on oxidative stress [4,12], although the effect of single administration is unknown. Therefore, immunohistochemistry was conducted in animals not dosed with CmP. Seven control mice (three were 5 weeks old and four were 8 weeks old), seven hepatic steatosis mice (all 5 weeks old), six steatohepatitis (NAS of 2) mice (all 5 weeks old), and eight steatohepatitis (NAS of 3) mice (four were 5 weeks old and four were 8 weeks old) were subjected to immunohistochemical examination.

After deparaffinization, sections were subjected to heat-mediated antigen retrieval using pH 6.0 citrate buffer within a pressure chamber for 10 min, blocking solution A (Histofine mouse stain kit, Nichirei Biosciences Inc., Tokyo, Japan) for 30 min to block non-specific binding, mouse monoclonal anti-4HNE (clone: HNEJ-2) at 1:75 dilution in IMMUNO SHOT Immunostaining, Fine (Cosmo Bio, Tokyo, Japan) for 30 min at room temperature, incubated in 3 % H_2O_2 for 5 min to block endogenous peroxidase activity, and incubated with blocking solution B (Histofine mouse stain kit, Nichirei Biosciences Inc., Tokyo, Japan) for 10 min to block nonspecific binding again. A simple stain, mouse MAX-PO(M) (Histofine mouse stain kit, Nichirei Biosciences Inc., Tokyo, Japan), which is a peroxidase-labeled anti-mouse IgG polyclonal antibody, was placed on the slides for 10 min. The slides were exposed to the 3.3'-diaminobenzidine for detection of specific immunolabeling. Sections were counterstained with hematoxylin.

Each entire histopathology slide with immunohistochemically stained tissue section was scanned with an Aperio AT2 whole digital slide scanner. Immunostaining positive area ratio was measured by HALO™ digital image analysis software version 3.4.2986.209 (Indicalabs, Corrales, NM, USA) using the CytoNuclear algorithm.

2.6. Statistics

The differences in the group means between multiple groups were statistically analyzed using Dunnett's test. The difference in the two groups means were statistically analyzed using Student's t test in the case of equal variance in F test, and Welch's test in the case of unequal variance in F test. All statistical analyzes were conducted by SAS version 9.4 software (SAS Institute Inc., Cary, NC, USA). P value < 0.05 was considered to indicate a significant difference.

3. Results

3.1. Phantom

The mean CNR was 8.500 ± 0.960 at 1 mM of CmP and was apparently distinguishable from background at ≥ 1 mM of CmP (Fig. 2A and B).

3.2. Histopathological examination

3.2.1. HE

In 5-week-old STAM™ mice evaluated by MRI, hepatic steatosis in 8/13 mice, steatohepatitis (NAS of 2) in 3/13 mice, and steatohepatitis (NAS of 3) in 2/13 mice were observed. In 8-week-old STAM™ mice evaluated by MRI, hepatic steatosis in 1/6 mice and steatohepatitis (NAS of 3) in 4/6 mice were observed (Fig. 3A–C). The remaining one mouse showed focal hyperintensity of the liver on T2-weighted MRI (Supplemental Fig. 1A). In that mouse, steatohepatitis (NAS = 6) at the same site of hyperintensity in T2-weighted MRI and steatohepatitis (NAS of 3) at the other site of the liver were observed (Supplemental Fig. 1B, C). Vacuolation in the hepatocytes and inflammatory cell infiltration were observed in all steatohepatitis, and ballooning was also observed in steatohepatitis (NAS of $\geq$3). Fibrosis was not observed in any STAM™ mice. In SAF-A score, steatohepatitis (NAS of 2) in 5-week-old STAM™ mice, steatohepatitis (NAS of 3) in 5-week-old STAM™ mice, and steatohepatitis (NAS of 3) in 8-week-old STAM™ mice were 1, 2, and 3, respectively. In 5- and 8-week-old control mice, no abnormal findings were observed in the liver (Fig. 3D). In the stomach, no abnormal findings were observed in any mouse for which a reduction rate could be calculated.

3.2.2. Immunohistochemistry

In the hepatic steatosis group, immunolabeling of 4-HNE in the cytoplasm of hepatocytes and/or mononuclear cells was observed with low frequency (Fig. 4A). In the steatohepatitis group, immunolabeling of 4-HNE in the cytoplasm was observed with high frequency in mononuclear cells and sometimes observed in hepatocytes (Fig. 4B and C). In the control group, no immunolabeling of 4-HNE was observed (Fig. 4D). In image analysis, the 4-HNE positive area ratio in the steatohepatitis (NAS of 3) group was significantly higher than that in other groups (Fig. 4E).

3.3. Reduction rate

In all STAM™ mice and control mice, hyperintensity of the liver in T1-weighted MRI was observed after CmP dosing. The signal intensity due to CmP gradually decayed, and at 15 min after CmP dosing, the signal intensity was comparable to that before administration (Fig. 5A). Images showing the reduction rate for each pixel in representative mice revealed that reduction rate in the whole area of the steatohepatitis group was higher than that in the whole area of the control and hepatic steatosis groups (Fig. 5B). Fig. 5C presents the typical signal intensity

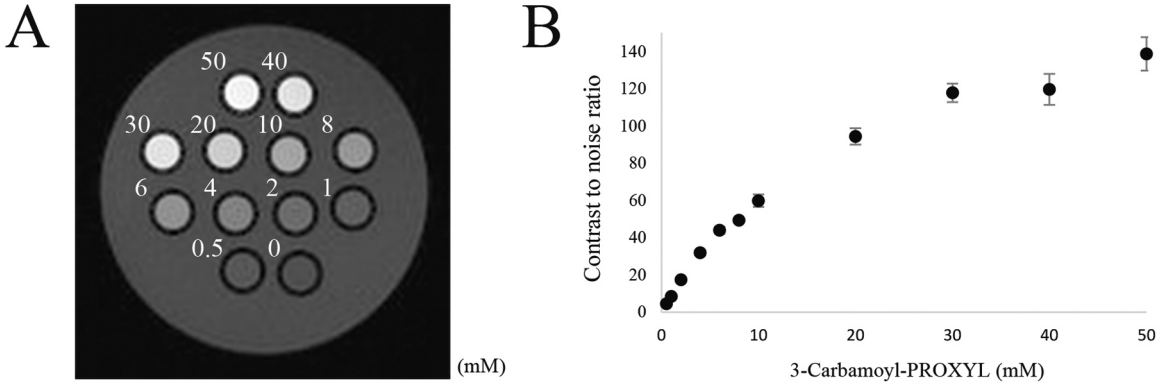

Fig. 2. Phantom images. (A) T1-weighted phantom image with 3-Carbamoyl-PROXYL (0–50 mM). (B) The mean contrast to noise ratios (CNRs) increased with increasing dose. The doses plotted are the same as in A. The mean CNRs at ≥ 1 mM exceeded 5 and meets the definition that is apparently distinguishable from background.

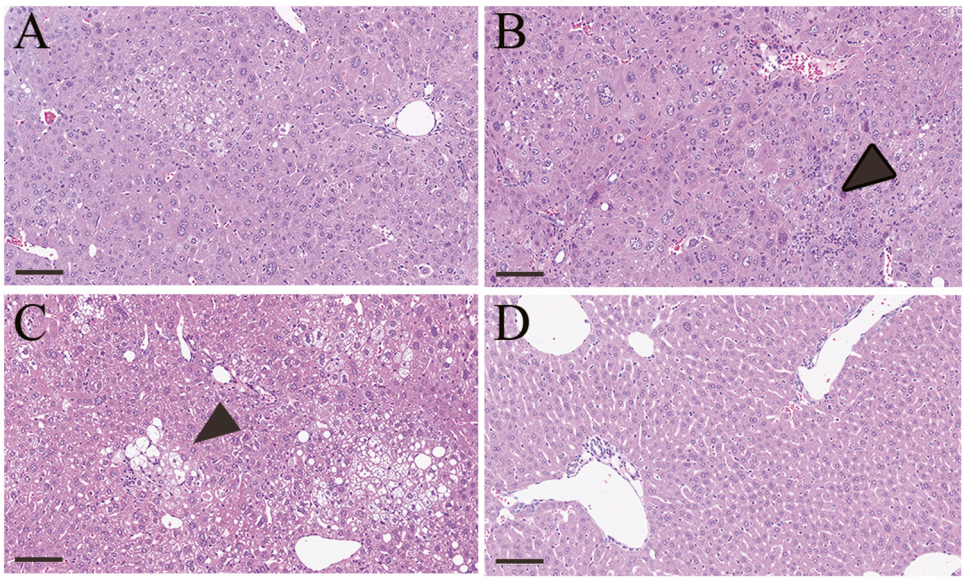

Fig. 3. Histopathological images in the liver. (A, B, C, and D) Typical histopathological images in the hepatic steatosis group (A), steatohepatitis (NAS of 2) group (B), steatohepatitis (NAS of 3) group (C), and control group (D). Vacuolation in hepatocytes is observed in the hepatic steatosis and steatohepatitis groups. Ballooning cells and/or inflammatory cells are indicated by black arrowheads. Bar, 100 μm.

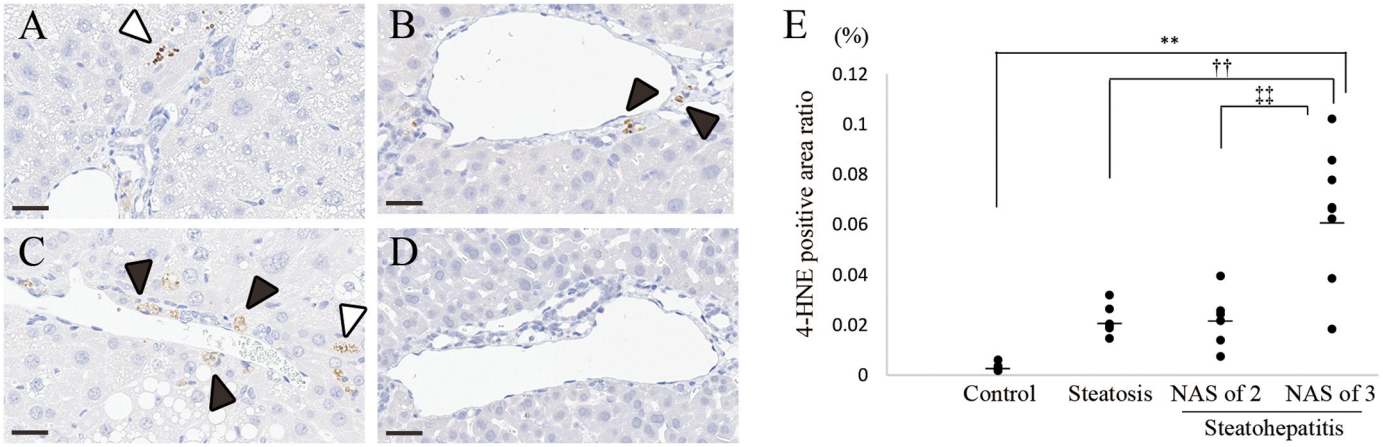

Fig. 4. 4-hydroxynoneal (4-HNE) immunolabeling and analysis in the liver. (A, B, C, and D) Typical immunohistochemical images of 4-HNE in the hepatic steatosis group (A), steatohepatitis (NAS of 2) group (B), steatohepatitis (NAS of 3) group (C), and control group (D). Immunolabeling of 4-HNE in the cytoplasm is indicated by white arrowheads in hepatocytes and black arrowheads in mononuclear cells. Bar, 30 μm. (E) Comparison of the 4-HNE positive area ratio in the steatohepatitis (NAS of 3) group to that in other groups. Significantly different from the control group: **$p < 0.01$, from the hepatic steatosis group: †† $p < 0.01$, and from the steatohepatitis group (NAS of 2): ‡‡ $p < 0.01$ (Dunnett's test). Bars indicate the mean values.

change rate of the liver in the control, hepatic steatosis, and steatohepatitis (NAS of 3) groups. The reduction rate in the liver was significantly higher in the steatohepatitis (NAS of 3) group than in other groups (Fig. 5D). In addition, the reduction rate in the liver tended to be higher as NAS increased from 2 to 3–6. According to the SAF-A score, the reduction rate in the liver was significantly higher in the steatohepatitis (SAF-A = 3) group than in the control, hepatic steatosis, and steatohepatitis (SAF-A = 1) groups (Supplemental Fig. 1). The steatohepatitis (SAF-A = 2) group was excluded from the statistical analysis since the number of data was two. The reduction rate in the liver tended to be higher as SAF-A score increased. In one 8-week-old STAM™ mouse, the reduction rate at the site showing hyperintensity in T2-weighted images was higher than that at the other site, and this site showing hyperintensity had the histopathological features of steatohepatitis (NAS of 6) in HE stained sections whereas the other site had the features of steatohepatitis (NAS of 3) (Supplemental Fig. 2A–D). In the image showing the reduction rate for each pixel, there was also a tendency for the reduction rate to be faster in area of hyperintensity in T2-weighted MRI (Supplemental Fig. 2E). No statistically significant difference in the reduction rate in the liver was observed between the control group and steatohepatitis (NAS of 2) group or between the hepatic steatosis group and steatohepatitis (NAS of 2) group.

In the reduction rate in the stomach, no statistically significant difference was observed between the control group and the other groups or between the hepatic steatosis group and steatohepatitis (NAS of 3) group (Fig. 6).

No differences in AUC were observed in the control liver, steatohepatitic liver (NAS of 3), and steatohepatitic liver (NAS of 6) in any interval (Supplemental Fig. 3).

3.4. *In vivo safety of CmP*

In blood biochemistry, no statistically significant difference was observed between the vehicle group and the CmP 200 mg/kg group

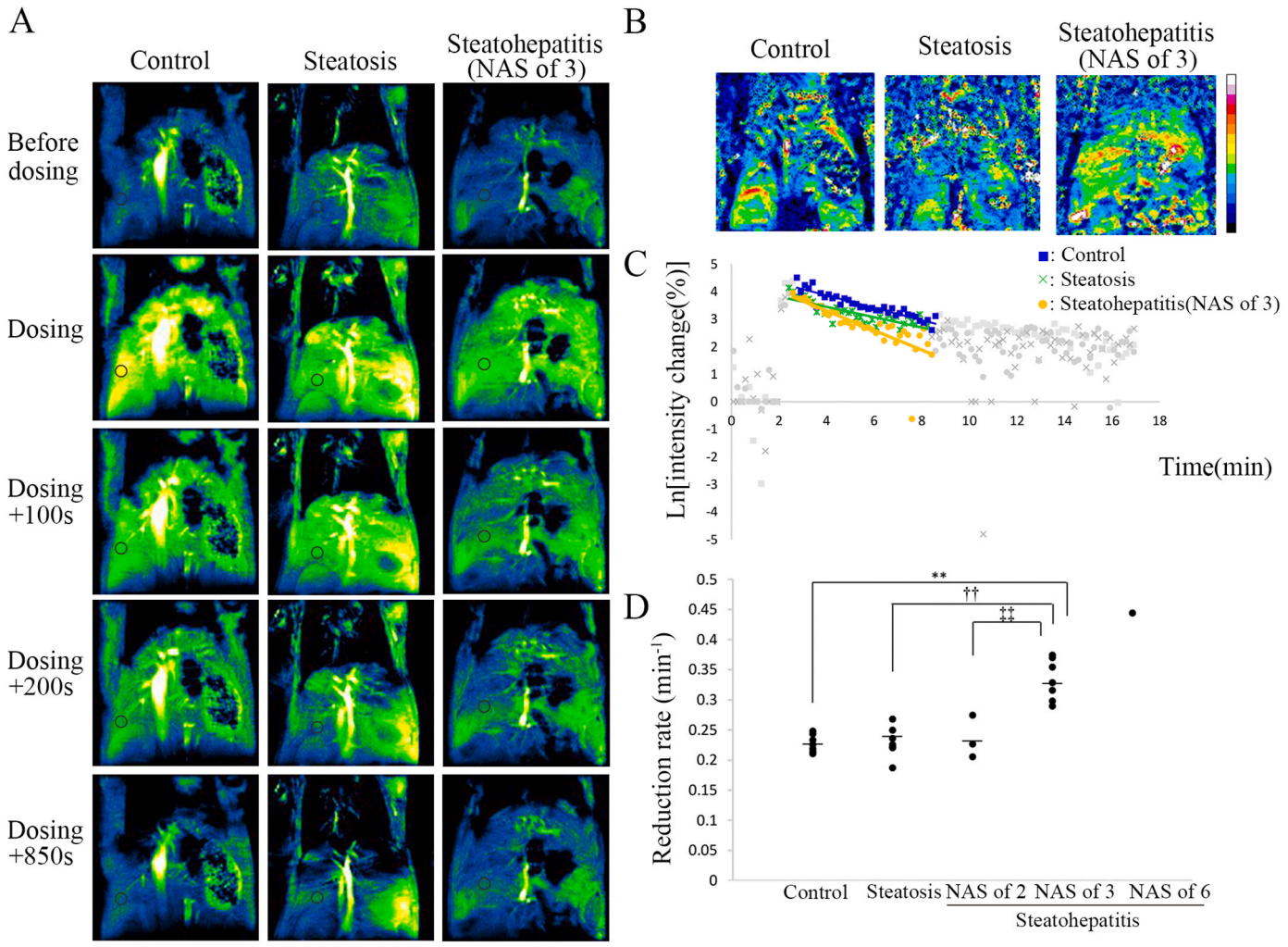

Fig. 5. T1-weighted sequential images with 3-Carbamoyl-PROXYL (CmP) and its analysis in the liver. (A) Typical T1-weighted sequential images with CmP. From the left, images are of the control liver, steatotic liver, and steatohepatitic liver (NAS of 3). Circle indicates region of interest. Hyperintensity of the liver in T1-weighted MRI was lost earlier in the steatohepatitic liver (NAS of 3) than in the control liver and steatotic liver. (B) Images show the reduction rate per pixel for three mice in A. White and black, the extremes of the color spectrum, represent the highest and lowest reduction rate, respectively. The color of the whole liver is mostly yellowish green in the steatohepatitic liver (NAS of 3), while it is mostly light blue in the control liver and steatotic liver. It showed that the reduction rate in the steatohepatitic liver (NAS of 3) was higher than in the other two. (C) The graph shows the sequential signal intensity change rate in the liver. Semilogarithmic plots of signal intensity change rate in the control liver (squares), steatotic liver (crosses), and steatohepatitic liver (NAS of 3; circles). The reduction rate was obtained from the slope of the linear regression line, and the range of data used for analysis is indicated by blue, green, and yellow dot plots. The graph shows that the slope was higher in steatohepatitic liver (NAS of 3) than in the control liver and steatotic liver. (D) The vertical dot plot shows a significantly higher reduction rate in the liver in the steatohepatitis (NAS of 3) group than in other groups. Significantly different from the control group: **$p < 0.01$, from the hepatic steatosis group: †† $p < 0.01$, and from the steatohepatitis group (NAS of 2): ‡‡ $p < 0.01$ (Dunnett's test). Bars indicate the mean values.

(Supplemental Table 1). In histopathology, no abnormal findings were observed in the liver, kidney, heart, lung, brain and administration site (tail) of any mice.

4. Discussion

To the best of our knowledge, this is the first report to show that the reduction rate measured by MRI was enhanced in the steatohepatitis mouse model compared to the hepatic steatosis mouse model. It suggests that steatohepatitis might be noninvasively differentiated from hepatic steatosis using CmP as an MRI contrast agent and the direction of the reduction rate in steatohepatitis was different in the models.

In the phantom study, ≥ 1 mM of CmP was apparently distinguishable from background. Since the maximum CmP concentration in the liver at the planned dose, 200 mg/kg, was predicted to be approximately 9 mM for the reason described below, it was assumed before conducting animal study that 200 mg/kg of CmP would provide sufficient signal enhancement in mouse livers, with images taken before dosing distinguishable from those taken after dosing. The maximum CmP concentration in the liver was predicted using the following procedure. In the CmP blood concentration simulation (intravenous injection) study, the initial distribution volume was three times the plasma volume [26], indicating that CmP is distributed in tissues immediately after dosing. Hypothesizing that CmP is uniformly distributed in all tissues, the maximum CmP concentration in the liver would be equivalent to the blood CmP concentration immediately after dosing. Therefore, the maximum CmP concentration in the liver at 200 mg/kg was calculated to be approximately 9 mM. The circulating blood volume of a mouse has been previously reported [9].

In immunohistochemistry, labeling of 4-HNE in the cytoplasm of hepatocytes and/or mononuclear cells was observed in the hepatic steatosis and steatohepatitis groups. In image analysis, the 4-HNE positive area ratio was significantly higher in the steatohepatitis (NAS of 3) group than the other groups, indicating that ROS was excessively

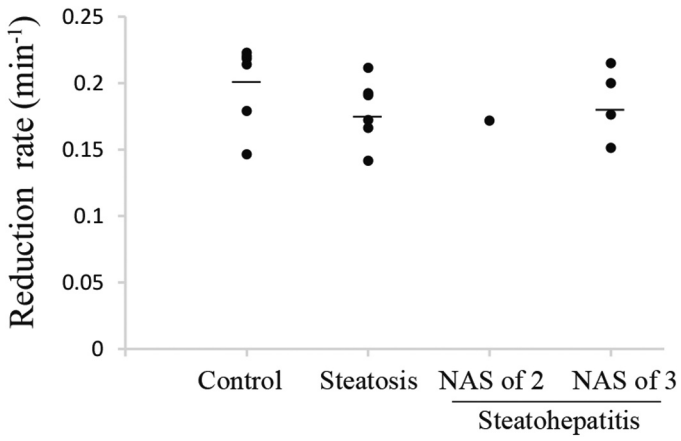

Fig. 6. Reduction rate in the stomach. The vertical dot plot shows that no statistically significant difference was observed in the reduction rate in the stomach between the control group and the other groups or between the hepatic steatosis group and steatohepatitis (NAS of 3) group. Bars indicate the mean values.

generated in steatohepatitis (NAS of 3) in STAM™ mice. Excess ROS has been reported previously in 12-week-old STAM™ mice showing steatohepatitis [17], but to the best of our knowledge, this is the first report to show that ROS was also excessively generated in 5- and 8-week-old STAM™ mice showing steatohepatitis (NAS of 3). Similar to the deposition pattern of 4-HNE in STAM™ mice, the 4-HNE immunolabel was observed in hepatocytes in hepatic steatosis and NASH patients [34,39] and in sinusoidal cells in NASH patients [39], suggesting that the disease in STAM™ mice may resemble human hepatic steatosis and NASH. Although the STAM™ mouse is not a model of drug-induced steatohepatitis, ROS excess develops in both drug-induced steatohepatitis and this model [1,23], suggesting that the present results could be extrapolated to drug-induced steatohepatitis.

In MRI examination using mice, the reduction rate in the liver was significantly higher in the steatohepatitis (NAS of 3) group than in other groups. In addition, images constructed from the reduction rate of each pixel indicated that the reduction rate calculated from the ROI was a representative value for the whole liver of each individual. The high reduction rate of MRI signal intensity reflects the fast conversion of the nitroxyl radical to the diamagnetic state. As discussed below, this high reduction rate was considered to be due to the difference in redox reaction. In the present study, excess ROS in steatohepatitis (NAS of 3) was indicated by higher 4-HNE positive area ratio. Therefore, the higher reduction rate in steatohepatitis (NAS of 3) was suggested to be due to excess ROS. This result was consistent with previous reports that the decay rates of nitroxyl radicals was enhanced in conditions associated with excessive ROS such as gastric ulcers, septic condition of the head, and focal muscle inflammation [13,14,43]. In addition, steatohepatitis (NAS of 3) is considered to be an early lesion, not yet a NASH lesion. From the above, it was indicated that CmP used as an MRI contrast agent has the potential to differentiate between early steatohepatitis and normal liver or hepatic steatosis based on the accumulation of excess ROS. To the best of our knowledge, this is the first report to show this result. Unlike ESR and DNP-MRI, MRI is widely used in both clinical and non-clinical studies. The method using MRI in the present study was more translational than these previous methods. Patients with drug-induced steatohepatitis will recover with drug withdrawal in many clinical cases [30,35]. However, if a chronic inflammatory state persists, drug-induced steatohepatitis may progress to cirrhosis eventually requiring liver transplantation [5,44]. Therefore, the present method, which has the potential to detect early steatohepatitis noninvasively and help determine whether drug withdrawal is necessary, was considered to be useful for drug development. Further studies with other animal models are warranted to verify the usefulness of the present method. Furthermore, data on the reduction rate in steatohepatitis (NAS of 6) was obtained from one animal, and it was observed that the reduction rate tended to increase with an increase in NAS. Therefore, it was suggested that the present method might be able to noninvasively detect the severity of steatohepatitis.

One STAM™ mouse showed focal hyperintensity in the liver in T2-weighted MRI, higher reduction rate in the focal hyperintensity site than in other liver sites in that mouse, and on histopathological examination, greater progression to steatohepatitis in the focal hyperintensity site than the other liver sites. These results suggest that the present method may be able to noninvasively detect differences in local lesion progression within the same individual. This was considered an advantage of MRI, which allows observation of the entire liver. Focal drug-induced steatosis and steatohepatitis have been reported in clinical studies [7,8]. Therefore, the present method of noninvasive detection of the local lesion progression within individuals may help clinicians monitor the occurrence and progression of local drug-induced steatohepatitis.

In the reduction rate in the stomach, no statistically significant difference was observed between the control group and the other groups, and between the hepatic steatosis group and steatohepatitis (NAS of 3) group. In addition, no histopathological abnormal findings in the stomach were observed in all control and STAM™ mice. These results suggested that the difference in the reduction rate in the liver was not due to the difference in systemic blood flow, and that the present method could specifically detect organs with excess ROS. CmP is repeatedly supplied to the liver because CmP remains in the circulating blood at least 30 min after dosing [26]. Therefore, the reduction rate is considered to be determined by supply of CmP to the tissue by blood flow, excretion of CmP from the tissue by blood flow, and redox reaction. No difference in gastric reduction rate between the control, hepatic steatosis, and steatohepatitis groups suggested that systemic blood flow was equivalent. Therefore, the difference in hepatic reduction rate was considered to be due to the difference in redox reaction, that is, the difference in ROS in the present study. In addition, the finding of no difference in AUC of Gd HP-DO3A between the control liver and steatohepatitic liver indicated the observation that the hepatic blood flow in control and model mice was also equivalent.

No statistically significant difference in the reduction rate and 4-HNE positive area ratio in the liver was observed between the steatohepatitis (NAS of 2) group and hepatic steatosis group and between the steatohepatitis (NAS of 2) group and control group, suggesting the absence of a statistically significant difference in hepatic ROS generation in these groups.

Nakata et al. has performed DNP-MRI with CmP in a NASH model induced by the MCD diet [29]. Unlike the findings of the present study, their research showed a significantly lower reduction rate in hepatic steatosis compared to control, and in steatohepatitis compared to both control and hepatic steatosis. In addition, oxidative stress was significantly elevated in the hepatic steatosis stage compared with the control. Nakata et al. thought that lipid peroxidation products produced by excess ROS inhibited complex IV in the mitochondrial electron transfer chain, and the inhibition of complex IV was associated with this lower reduction rate. Therefore, it was considered that different steatohepatitis-inducing mechanisms would change whether the redox balance is affected by ROS excess or mitochondrial complex IV inhibition and this difference would affect the reduction rate. Whatever mechanism is involved in steatohepatitis, it is considered that the degree of redox imbalance differs between steatohepatitis and hepatic steatosis, which is reflected as a significant difference in the reduction rate. Since the increase or decrease in the reduction rate in steatohepatitis in clinical studies could be predicted by confirming the direction of change in the reduction rate in preclinical studies, it was considered possible to differentiate between the two using the present method in clinical studies.

Drug-induced hepatic steatosis/steatohepatitis and NAFLD/NASH are two separate and distinct groups of entities. However, they share several similar histopathological and clinical features, which may suggest the existence of common biomarkers [31]. Several papers have reported candidate methods for differentiating NASH and simple steatosis using MRI. The hepatic levels of metabolites under anaerobic conditions produced by inflammation, quantified by ^{1}H-magnetic resonance spectroscopy, have been higher in NASH (NAS of $\geq$ 5) than in simple steatosis (NAS of $<$ 5) in humans and mice [19], and uptake of hepatic ultrasmall superparamagnetic iron oxide particles (USPIOs) in patients with NASH (NAS of $\geq$ 5) has been decreased compared with that in patients with simple steatosis (NAS of $<$ 5) and healthy controls, which is likely due to phagocytic dysfunction of Kupffer cells in NASH [40]. Compared to those previous methods, the present method relies on a different mechanism and stage of the lesion: excess ROS generation and early steatohepatitis. The present method, which detects early steatohepatitis by monitoring excess ROS generation, is considered to be useful for detecting drug-induced steatohepatitis. Drugs that induce steatohepatitis have been reported to largely have off-therapeutic target effects which cause mitochondrial damage leading to excess ROS [38]. Therefore, it is expected that the present method focusing on excess ROS may be useful in the detection of steatohepatitis induced by many types of drugs. In addition, the present method has the potential to detect steatohepatitis before it progresses to NASH. Early detection of steatohepatitis can help patients recover with drug withdrawal and prevent progression to more serious and potentially fatal findings. Furthermore, although their value has not yet been established, NASH blood biomarkers, such as plasma cytokeratin 18 and microRNAs, have been also reported [31,32]. Blood biomarkers reflect the condition in the whole body so that it was assumed that the present method might be better at monitoring local steatohepatitis than blood biomarkers.

There are two points to consider when using the present method clinically. The first point is about the clinical use of CmP. Nitroxyl radical had been applied topically to humans [28], but has not been approved as a clinical contrast agent. Although data showing the usefulness of nitroxyl radicals as a contrast agent has been accumulated, there are few reports verifying its safety. Therefore, we conducted the examination to verify the safety of CmP. When CmP was administered intravenously into rats, the signal intensity due to CmP in the heart, liver, kidney, and intestines declined gradually and reached the background level at 1000 s after administration [42]. In addition, the half-life of CmP in the blood, liver, and kidneys in mice has been reported to be less than 30 min [16,26]. Since these results suggest that CmP has a low bioaccumulation, we conducted the examination to verify the safety of the day after a single administration. In blood biochemistry and histopathology of principal organs and administration site, no CmP-related changes were observed. Further examination is required before CmP can be approved as a clinical contrast agent, but approval for clinical use could be expected in the future. The second point is detection in clinical MRI. 11.7T MRI was used in the present study because mice were small, but the static magnetic field strength of MRI is usually 3T or less. However, phantom containing 1 mM of CmP has been readily identifiable in 3T MRI [42]. Therefore, it might be possible to detect changes in reduction rate in human steatohepatitis using clinical MRI. Although NAS was used to express the severity of steatohepatitis in the present study, NAS is not necessarily used in humans either. However, since the reduction rate tended to increase with the score in SAF-A, it was expected that the present method might have the potential to detect early steatohepatitis regardless of the scoring methods. From the above, it was assumed that the present method has the potential to be used not only in non-clinical settings but also in clinical settings.

In conclusion, it was indicated that CmP used as an MRI contrast agent has the potential to organ-specifically differentiate between the early steatohepatitic liver and normal or steatosic liver based on ROS. ROS has been reported to be generated in drug-induced steatohepatitis in both humans and animals [1,10,22,23], warranting consideration of the present method as a candidate noninvasive method for differentiating between early drug-induced steatohepatitis and hepatic steatosis.

Funding

This work was supported by Sumitomo Pharma Co., Ltd.

CRediT authorship contribution statement

Izuru Miyawaki: Conceptualization, Supervision, Writing – review & editing. **Yoshichika Yoshioka:** Conceptualization, Investigation, Methodology, Supervision, Writing – review & editing. **Jun-ichiro Enmi:** Conceptualization, Formal analysis, Investigation, Methodology, Supervision, Visualization, Writing – review & editing. **Aya Nakae:** Conceptualization, Supervision, Writing – review & editing. **Kazuhiro Chihara:** Conceptualization, Supervision, Writing – review & editing. **Yuta Fujii:** Conceptualization, Investigation, Methodology, Writing – review & editing. **Yuka Yoshino:** Conceptualization, Formal analysis, Investigation, Methodology, Visualization, Writing – original draft.

Declaration of Competing Interest

The authors declare that they have no known competing financial interests or personal relationships that could have appeared to influence the work reported in this paper.

Data availability

Data will be made available on request.

Acknowledgements

We thank Mr. Y. Sasaki and Mr. K. Abe for their excellent technical assistance.

Authorship statement

All persons who meet authorship criteria are listed as authors, and all authors certify that they have participated sufficiently in the work to take public responsibility for the content, including participation in the concept, design, analysis, writing, or revision of the manuscript. Furthermore, each author certifies that this material or similar material has not been and will not be submitted to or published in any other publication before its appearance in Toxicology Reports.

Appendix A. Supporting information

Supplementary data associated with this article can be found in the online version at doi:10.1016/j.toxrep.2023.12.002.

References

[1] H.M. Abo-Haded, M.A. Elkablawy, Z. Al-Johani, O. Al-Ahmadi, D.S. El-Agamy, Hepatoprotective effect of sitagliptin against methotrexate induced liver toxicity, PLoS One 12 (3) (2017), e0174295.
[2] D.E. Amacher, Strategies for the early detection of drug-induced hepatic steatosis in preclinical drug safety evaluation studies, Toxicology 279 (1–3) (2011) 10–18.
[3] Y. Ando, J.H. Jou, Nonalcoholic fatty liver disease and recent guideline updates, Clin. Liver Dis. 17 (1) (2021) 23–28.
[4] M. Assayag, S. Goldstein, A. Samuni, N. Berkman, 3-Carbamoyl-proxyl nitroxide radicals attenuate bleomycin-induced pulmonary fibrosis in mice, Free Radic. Biol. Med. 171 (2021) 135–142.
[5] C. Berardo, L.G. Di Pasqua, M. Cagna, P. Richelmi, M. Vairetti, A. Ferrigno, Nonalcoholic fatty liver disease and non-alcoholic steatohepatitis: current issues and future perspectives in preclinical and clinical research, Int. J. Mol. Sci. 21 (24) (2020) 9646.
[6] A.E. Bohte, J.R. van Werven, S. Bipat, J. Stoker, The diagnostic accuracy of US, CT, MRI and ^{1}H-MRS for the evaluation of hepatic steatosis compared with liver biopsy: a meta-analysis, Eur. Radiol. 21 (1) (2011) 87–97.

[7] L. Calistri, V. Rastrelli, C. Nardi, D. Maraghelli, S. Vidali, M. Pietragalla, S. Colagrande, Imaging of the chemotherapy-induced hepatic damage: Yellow liver, blue liver, and pseudocirrhosis, World J. Gastroenterol. 27 (46) (2021) 7866–7893.
[8] J.S. Choi, M.J. Kim, Education and imaging: hepatobiliary and pancreatic: focal steatohepatitis mimicking a metastasis, J. Gastroenterol. Hepatol. 26 (2) (2011) 415.
[9] K.H. Diehl, R. Hull, D. Morton, R. Pfister, Y. Rabemampianina, D. Smith, J. M. Vidal, C. van de Vorstenbosch, European Federation of Pharmaceutical Industries Association and European Centre for the Validation of Alternative Methods, A good practice guide to the administration of substances and removal of blood, including routes and volumes, J. Appl. Toxicol. 21 (1) (2001) 15–23.
[10] M.T. Donato, A. Martínez-Romero, N. Jiménez, A. Negro, G. Herrera, J.V. Castell, J.E. O'Connor, M.J. Gómez-Lechón, Cytometric analysis for drug-induced steatosis in HepG2 cells, Chem. Biol. Interact. 181 (3) (2009) 417–423.
[11] J.C. Duvigneau, A. Luís, A.M. Gorman, A. Samali, D. Kaltenecker, R. Moriggl, A. V. Kozlov, Crosstalk between inflammatory mediators and endoplasmic reticulum stress in liver diseases, Cytokine 124 (2019), 154577.
[12] A. Eguchi, T. Yoshitomi, M. Lazic, C.D. Johnson, L.B. Vong, A. Wree, D. Povero, B. G. Papouchado, Y. Nagasaki, A.E. Feldstein, Redox nanoparticles as a novel treatment approach for inflammation and fibrosis associated with nonalcoholic steatohepatitis, Nanomedicine 10 (17) (2015) 2697–2708.
[13] H. Eto, F. Hyodo, N. Kosem, R. Kobayashi, K. Yasukawa, M. Nakao, M. Kiniwa, H. Utsumi, Redox imaging of skeletal muscle using in vivo DNP-MRI and its application to an animal model of local inflammation, Free Radic. Biol. Med. 89 (2015) 1097–1104.
[14] H.G. Fujii, H. Sato-akaba, M.C. Emoto, K. Itoh, Y. Ishihara, H. Hirata, Noninvasive mapping of the redox status in septic mouse by in vivo electron paramagnetic resonance imaging, Magn. Reson. Imaging 31 (1) (2013) 130–138.
[15] M. Fujii, Y. Shibazaki, K. Wakamatsu, Y. Honda, Y. Kawauchi, K. Suzuki, S. Arumugam, K. Watanabe, T. Ichida, H. Asakura, H. Yoneyama, A murine model for non-alcoholic steatohepatitis showing evidence of association between diabetes and hepatocellular carcinoma, Med. Mol. Morphol. 46 (3) (2013) 141–152.
[16] A. Hirayama, K. Yoh, S. Nagase, A. Ueda, K. Itoh, N. Morito, K. Hirayama, S. Takahashi, M. Yamamoto, A. Koyama, EPR imaging of reducing activity in Nrf2 transcriptional factor-deficient mice, Free Radic. Biol. Med. 34 (10) (2003) 1236–1242.
[17] H. Ishikawa, A. Takaki, R. Tsuzaki, T. Yasunaka, K. Koike, Y. Shimomura, H. Seki, H. Matsushita, Y. Miyake, F. Ikeda, H. Shiraha, K. Nouso, K. Yamamoto, L-Carnitine prevents progression of non-alcoholic steatohepatitis in a mouse model with upregulation of mitochondrial pathway, PLoS One 9 (7) (2014), e100627.
[18] R. Kerlin, B. Bolon, J. Burkhardt, S. Francke, P. Greaves, V. Meador, J. Popp, Scientific and regulatory policy committee: recommended ("Best") practices for determining, communicating, and using adverse effect data from nonclinical studies, Toxicol. Pathol. 44 (2) (2016) 147–162.
[19] T.H. Kim, H.Y. Jun, K.J. Kim, Y.H. Lee, M.S. Lee, K.H. Choi, K.J. Yun, Y.Y. Jeong, C. H. Jun, E.Y. Cho, K.H. Yoon, Hepatic alanine differentiates nonalcoholic steatohepatitis from simple steatosis in human and mice: a proton MR spectroscopy study with ling echo time, J. Magn. Reson. Imaging 46 (5) (2017) 1298–1310.
[20] D.E. Kleiner, E.M. Brunt, M. Van Natta, C. Behling, M.J. Contos, O.W. Cummings, L. D. Ferrell, Y.C. Liu, M.S. Torbenson, A. Unalp-Arida, M. Yeh, A.J. McCullough, A. J. Sanyal, Nonalcoholic steatohepatitis clinical research network. Design and validation of a histological scoring system for nonalcoholic fatty liver disease, Hepatology 41 (6) (2005) 1313–1321.
[21] T.O. Kolaric, V. Nincevic, L. Kuna, K. Duspara, K. Bojanic, S. Vukadin, N. Raguz-Lucic, G.Y. Wu, M. Smolic, Drug-induced fatty liver disease: pathogenesis and treatment, J. Clin. Transl. Hepatol. 9 (5) (2021) 731–737.
[22] B. Liu, C. Ding, W. Tang, C. Zhang, Y. Gu, Z. Wang, T. Yu, Z. Li, Hepatic ROS mediated macrophage activation is responsible for irinotecan induced liver injury, Cells 11 (23) (2022) 3791.
[23] Y. Lu, Y. Lin, X. Huang, S. Wu, J. Wei, C. Yang, Oxaliplatin aggravates hepatic oxidative stress, inflammation and fibrosis in a non-alcoholic fatty liver disease mouse model, Int. J. Mol. Med. 43 (6) (2019) 2398–2408.
[24] Y. Ma, G. Lee, S.Y. Heo, Y.S. Roh, Oxidative stress is a key modulator in the development of nonalcoholic fatty liver disease, Antioxidants 11 (1) (2021) 91.
[25] A. Matsumoto, K. Matsumoto, S. Matsumoto, F. Hyodo, A.L. Sowers, J. W. Koscielniak, N. Devasahayam, S. Subramanian, J.B. Mitchell, M.C. Krishna, Intracellular hypoxia of tumor tissue estimated by noninvasive electron paramagnetic resonance oximetry technique using paramagnetic probes, Biol. Pharm. Bull. 34 (1) (2011) 142–145.
[26] K. Matsumoto, M.C. Krishna, J.B. Mitchell, Novel pharmacokinetic measurement using electron paramagnetic resonance spectroscopy and simulation of in vivo decay of various nitroxyl spin probes in mouse blood, J. Pharmacol. Exp. Ther. 310 (3) (2004) 1076–1083.
[27] K. Matsumoto, F. Hyodo, A. Matsumoto, A.P. Koretsky, A.L. Sowers, J.B. Mitchell, M.C. Krishna, High-resolution mapping of tumor redox status by magnetic resonance imaging using nitroxides as redox-sensitive contrast agents, Clin. Cancer Res. 12 (8) (2006) 2455–2462.
[28] J.M. Metz, D. Smith, R. Mick, R. Lustig, J. Mitchell, M. Cherakuri, E. Glatstein, S. M. Hahn, A phase I study of topical Tempol for the prevention of alopecia induced by whole brain radiotherapy, Clin. Cancer Res. 10 (19) (2004) 6411–6417.
[29] R. Nakata, F. Hyodo, M. Murata, H. Eto, T. Nakaji, T. Kawano, S. Narahara, K. Yasukawa, T. Akahoshi, M. Tomikawa, M. Hashizume, In vivo redox metabolic imaging of mitochondria assesses disease progression in non-alcoholic steatohepatitis, Sci. Rep. 7 (1) (2017), 17170.
[30] V. Patel, A.J. Sanyal, Drug-induced steatohepatitis, Clin Liver Dis. 17 (4) (2013) 533–546.
[31] L. Pavlik, A. Regev, P.A. Ardayfio, N.P. Chalasani, Drug-induced steatosis and steatohepatitis: The search for novel serum biomarkers among potential biomarkers for non-alcoholic fatty liver disease and non-alcoholic steatohepatitis, Drug Saf. 42 (6) (2019) 701–711.
[32] V.A. Piazzolla, A. Mangia, Noninvasive diagnosis of NAFLD and NASH, Cells 9 (4) (2020) 1005, 17.
[33] C.J. Pirola, M. Garaycoechea, D. Flichman, G.O. Castaño, S. Sookoian, Liver mitochondrial DNA damage and genetic variability of Cytochrome b - a key component of the respirasome - drive the severity of fatty liver disease, J. Intern. Med. 289 (1) (2021) 84–96.
[34] M.C. Podszun, J.Y. Chung, K. Ylaya, D.E. Kleiner, S.M. Hewitt, Y. Rotman, 4-HNE immunohistochemistry and image analysis for detection of lipid peroxidation in human liver samples using vitamin E treatment in NAFLD as a proof of concept, J. Histochem. Cytochem. 68 (9) (2020) 635–643.
[35] R. Ramachandran, S. Kakar, Histological patterns in drug-induced liver disease, J. Clin. Pathol. 62 (6) (2009) 481–492.
[36] A. Rose, The sensitivity performance of the human eye on an absolute scale, J. Opt. Soc. Am. 38 (1948) 196–208.
[37] S.K. Satapathy, V. Kuwajima, J. Nadelson, O. Atiq, A.J. Sanyal, Drug-induced fatty liver disease: An overview of pathogenesis and management, Ann. Hepatol. 14 (6) (2015) 789–806.
[38] J.D. Schumacher, G.L. Guo, Mechanistic review of drug-induced steatohepatitis, Toxicol. Appl. Pharmacol. 289 (1) (2015) 40–47.
[39] S. Seki, T. Kitada, T. Yamada, H. Sakaguchi, K. Nakatani, K. Wakasa, In situ detection of lipid peroxidation and oxidative DNA damage in non-alcoholic fatty liver diseases, J. Hepatol. 37 (1) (2002) 56–62.
[40] L.P. Smits, B.F. Coolen, M.D. Panno, J.H. Runge, W.H. Nijhof, J. Verheij, M. Nieuwdorp, J. Stoker, U.H. Beuers, A.J. Nederveen, E.S. Stroes, Noninvasive differentiation between hepatic steatosis and steatohepatitis with MR imaging enhanced with USPIOs in patients with nonalcoholic fatty liver disease: a proof of concept study, Radiology 278 (3) (2016) 782–791.
[41] B.P. Soule, F. Hyodo, K. Matsumoto, N.L. Simone, J.A. Cook, M.C. Krishna, J. B. Mitchell, The chemistry and biology of nitroxide compounds, Free Radic. Biol. Med. 42 (11) (2007) 1632–1650.
[42] T. Uchida, H. Togashi, Y. Kuroda, K. Haga, M. Sadahiro, T. Kayama, In vivo visualization of redox status by high-resolution whole body magnetic resonance imaging using nitroxide radicals, J. Clin. Biochem. Nutr. 63 (3) (2018) 192–196.
[43] H. Utsumi, K. Yasukawa, T. Soeda, K. Yamada, R. Shigemi, T. Yao, M. Tsuneyoshi, Noninvasive mapping of reactive oxygen species by in vivo electron spin resonance spectroscopy in indomethacin-induced gastric ulcers in rats, J. Pharmacol. Exp. Ther. 317 (1) (2006) 228–235.
[44] Q. Wang, A. Huang, J.B. Wang, Z. Zou, Chronic drug-induced liver injury: updates and future challenges, Front. Pharmacol. 12 (2021), 627133.